*Pol. J. Environ. Stud. Vol. XX, No. X (XXXX), 1-17*
DOI: *10.15244/pjoes/214675* ONLINE PUBLICATION DATE: 2026-03-04

*Original Research*

# Integrated Hydrogeochemical Assessment of Groundwater Resources for Sustainable Management in the Southwest Dongping Lake Region

**Feng Zhang[1, 2, 3], Bin Gao[4], Chunying Xia[1, 2], Lei Ren[5], Yalei Yan[4], Hua Xiao[1, 2], Huiming Zheng[1, 2, 3°*]**

[1]Shandong Provincial Lunan Geology and Exploration Institute (Shandong Provincial Bureau of Geology and Mineral Resources No. 2 Geological Brigade), Jining 272100, China
[2]Shandong Engineering Research Center of Geothermal Energy Exploration and Development, Jining 272100, China
[3]Shandong Provincial Key Laboratory of Geothermal Clean Energy, Jining 272000, China
[4]Petro China Zhejiang Oil field Company Limited, Hangzhou 310023, China
[5]Liangshan County Natural Resources and Planning Bureau, Jining 272600, China

*Received: 11 July 2025*
*Accepted: 24 November 2025*

## Abstract

In order to characterize the groundwater characteristics in the southwestern region of Dongping Lake, statistics, Piper plot, Gibbs plot, and ion comparison were used to analyze 48 samples, evaluate the drinkability and irrigation suitability of groundwater in the SDLR area, and assess the human health risks associated with nitrate and fluoride pollution. The groundwater in the SDLR area is weakly alkaline, hard freshwater. Karst water shows the $SO_4$·Cl-Ca·Mg type, while pore water is mainly composed of $HCO_3$-Ca·Mg and $SO_4$·Cl-Ca·Mg. Rock weathering is mainly caused by carbonate dissolution, with a small amount of silicate and gypsum input being the main factors dominating the hydrochemical characteristics; cation exchange is also an important hydrochemical mechanism. All samples of $NO_3^-$ meet the Class III limit (≤88.6mg/L), mainly from feces and sewage. The evaluation of irrigation water quality shows that salinization is more harmful than alkalinity, and most water samples are suitable for irrigation. Poor quality water is limited to the north. The human health risk model shows that 60% of the samples pose a non-carcinogenic threat, with children being more affected than adults; oral intake is the main route. High-risk areas are concentrated in the north and southwest. The research results provide a scientific basis for sustainable groundwater management in SDLR.

**Keywords:** groundwater, major ions, hydrogeochemical signatures, quality assessment, the southwest Dongping Lake region

*e-mail: lnyzhenghm@163.com
°ORCID iD: 0009-0009-2247-0082

## Introduction

Groundwater offers numerous advantages, including its widespread distribution, excellent water quality, and low susceptibility to pollution [1, 2]. As a globally significant water source and strategic resource, groundwater fundamentally sustains urban domestic water supplies, underpins socioeconomic stability, and maintains ecological equilibrium [3-5]. The hydrogeochemical signature of groundwater is affected by multiple factors, including geology, hydrogeology, climate, land use patterns, and human activities[6]. During the runoff process, it continuously exchanges materials with the surrounding environment [7-9].

As the socio-economic landscape evolves rapidly, anthropogenic impacts on groundwater systems are becoming increasingly significant. Consequently, understanding the hydrogeochemical signatures of regional groundwater and identifying the factors that shape them is essential for sound governance and sustainable utilization of groundwater resources. For instance, Esmaeili Vardanjani et al. examined the formation of hydrochemical components in groundwater in the Kadkan Region of northeastern Iran [10]. Their findings indicate that geological conditions, mineral weathering and dissolution, and the ion composition of groundwater are the primary determinants of the hydrochemical composition in that area. Rosenthal et al. performed a systematic investigation of hydrochemical evolution processes in saline groundwater systems spanning the western Negev (Israel) and central northern Sinai (Egypt) regions [11]. They identified a significant correlation between groundwater salinization and natural factors, such as geological structures. Given the relatively slow natural runoff and self-renewal rates of groundwater, the likelihood of relying solely on natural recovery in the event of pollution is minimal. Consequently, it is imperative to conduct thorough testing and evaluation during the development and utilization of groundwater. Li et al. assessed the quality of groundwater in the Pinggu Basin of Beijing [12]. Their analysis demonstrated an Entropy Water Quality Index (EWQI) range of 25-141 across the basin, with over 50% of samples meeting Grade 1 or 2 classification standards. Geospatial assessment indicated that while southwestern and northwestern sectors exhibited substandard water quality, the majority of groundwater samples maintained potability thresholds suitable for human consumption. Pham and Nguyen employed multivariate statistical analysis and GWQI to assess groundwater quality in Gia Lai Province, Vietnam. Groundwater quality was categorized into four grades: excellent (44%), good (40%), poor (12%), and very poor (4%). Potential sources of groundwater variability include domestic and industrial wastewater discharge, landfill leachate from burial grounds, aquifer characteristics, and seawater intrusion [2]. Biswas et al. effectively assessed the suitability of groundwater for irrigation in their study area using USSL and Wilcox diagrams [13]. Conducting a health risk assessment is essential to safeguard human health from the impacts of pollutants. The United States Environmental Protection Agency (USEPA) has developed a method to evaluate the health risks posed by pollutants through ingestion, skin contact, and inhalation [14]. Long-term consumption of groundwater containing elevated nitrate concentrations has been associated with the development of methemoglobinemia, increased risk of gastrointestinal cancers, and various other negative health outcomes. In a health risk assessment of pollutants in Yan'an City, Shaanxi Province, it was determined that nitrate posed the highest non-carcinogenic risk, followed by fluoride [15]. Similarly, Din et al. found that drinking water containing fluoride and nitrate from various regions in Pakistan presents potential health risks through oral intake [16]. These risks are particularly pronounced in children compared to adults, with nitrate posing a greater risk than fluoride.

As a vital water resource in the Dongping Lake Basin, groundwater serves as an essential component supporting regional socio-economic progress. Current research on the hydrochemical characteristics of groundwater and their controlling factors in the Dongping Lake basin remains relatively limited. For instance, Zhao et al. performed a hydrogeochemical investigation examining groundwater composition and formation mechanisms in Liangshan County [17], Hu et al. evaluated the quality of Dongping Lake groundwater during the dry season using cloud models [18], and Qin et al. characterized the hydrogeochemical features and evaluated groundwater quality surrounding areas of Dongping Lake [19]. Despite these efforts, research on different types of groundwater in the SDLR remains limited. There has been little work to systematically couple the hydrochemical evolution mechanism of SDLR with the human health risks posed by nitrate and fluoride, and this gap urgently needs to be filled. Consequently, this study selected 48 groundwater samples from the southwestern area, comprising 8 karst water samples and 40 pore water samples. By employing statistical analysis and comprehensive hydrochemical methods, the study aims to elucidate the characteristics of groundwater hydrogeochemistry and analyze its influencing factors. This research will provide a scientific foundation for the sustainable exploitation, utilization, and governance of groundwater in SDLR.

## Study Area

The SDLR is located at the western edge of Shandong Province and the northwestern corner of Jining City (Fig. 1), which is situated in the bordering zone of two provinces and five prefectures (cities). The geographic coordinates are 115°51′37″~116°21′26″ east longitude and 35°36′36″~35°58′29″ north latitude. This district serves as a significant commercial grain production base county, characterized by deep, fertile soils, where arable

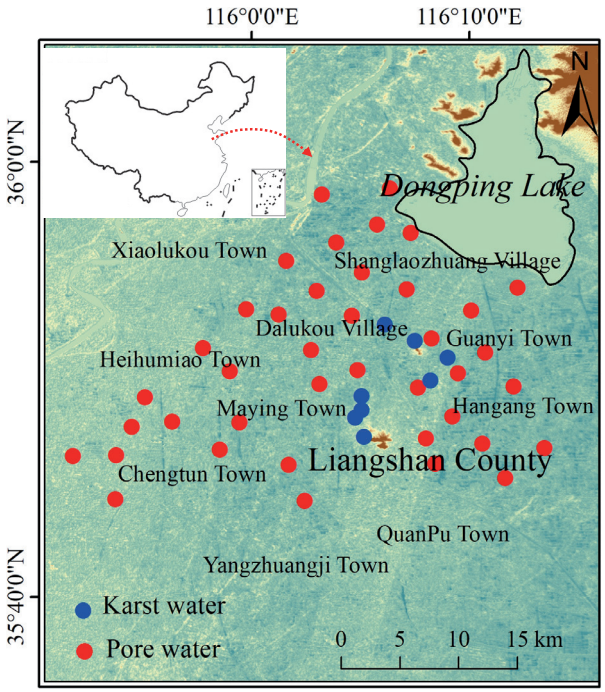


Fig. 1. Geographic distribution of sampling sites within the SDLR.

land predominates as the primary land use type (Fig. 2). Traffic is very convenient, with railway, highway, and water transport in the region. A comprehensive and more developed transport network for regional industrial and agricultural production provides convenient transport conditions. The area has a warm-temperate monsoon-type continental climate, with four distinct seasons, rain and heat at the same time, frequent droughts, and floods. In the SDLR, the water system is well-developed. With the exception of the Yellow River beach area, which falls within the Yellow River Basin, the remainder of the region is part of the Huaihe River Basin. The Yellow River is adjacent to the northern part of the area, and there are irrigation canals all over the area, while the Beijing-Hangzhou Canal runs through the middle of the SDLR in a north-west-south-east direction, intersects with other rivers in the area, and flows into Nansihu to the south of SDLR. The SDLR is located in the western part of the Luzhong mountainous area on the edge of the Taishan Mountains, which is the edge of the transition from the Luzhong mountainous area to the North China Plain, and is situated in the superposition zone of the Yellow River alluvial deposits and the Wensi River alluvial deposits, which is the confluence of the east and west waters. There are mountains, rivers, lakes, dykes, and plains in the territory, and the terrain is gentle, high in the north-west and low in the south-east.

Based on the occurrence conditions, hydraulic connections, and stratigraphic and lithological relationships of groundwater in the study area, aquifers can be categorized into three types: loose rock pore aquifers, carbonate rock fracture-karst aquifers, and other aquifers. Quaternary loose deposits, which are extensively distributed throughout the area, include the Wen River and Yellow River alluvial deposits. These loose rock pore waters constitute the main water source in SDLR. Karst water in carbonate rock fissures is predominantly found in the Xiao'an Mountain area of Liangshan in the north. The lithology primarily consists

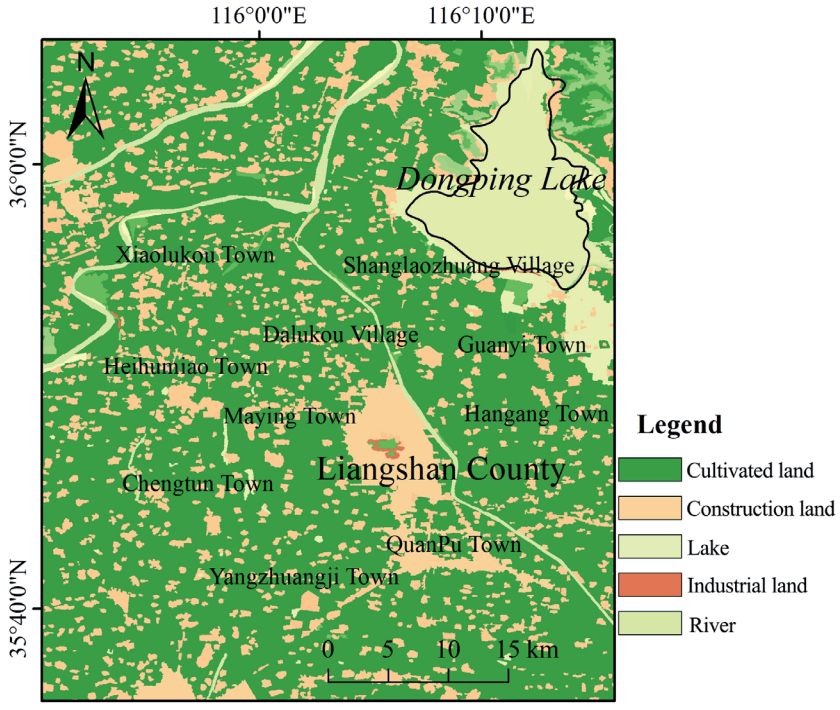


Fig. 2. Land use situation in SDLR.

of limestone, mudstone, dolomite, and dolomitic limestone from the Middle and Upper Cambrian and Ordovician periods. The presence of extensive rock strata and developed karst fissure networks creates optimal hydrogeological conditions for groundwater storage and circulation, leading to substantial groundwater reserves.

Groundwater movement in the region is influenced by geological structures, topography, meteorological conditions, hydrological factors, and human activities. Shallow pore water is primarily affected by meteorological and hydrological factors, whereas deep pore water and fracture-karst water are predominantly controlled by geological structures. The sources of pore water include atmospheric precipitation, lateral infiltration from the Yellow River, infiltration from channel water, and irrigation seepage. The primary discharge method is artificial extraction, followed by evaporation. Fracture-karst water is mainly recharged through lateral groundwater runoff, supplemented by atmospheric precipitation and overflow from upper Quaternary pore water. The sole discharge pathway for karst water is artificial extraction, which is predominantly found in shallow areas around Liangshan County. It is primarily used for industrial production and urban domestic water supply.

## Materials and Methods

### Collecting and Testing

For this research, 48 samples were systematically obtained during March 2023. Among them, there are 8 karst water samples and 40 pore water samples, and the geographical positions of the sample points are depicted in Fig. 1. During the sampling process, the wells were pre-pumped for 10 minutes before sampling to ensure that fresh groundwater samples were obtained. Sampling was conducted using four sterile polyethylene containers, each rinsed thoroughly (≥3 times) with native groundwater prior to final sample collection. During the collecting process, the water flowed slowly into the sampling bottles until they were completely filled, then the caps were tightened and sealed. After sampling, samples were immediately refrigerated during storage and transportation to ensure preservation, with expedited delivery to the laboratory for subsequent water quality analyses.

The water samples were tested by the Experimental Testing Centre of Lunan Geological Engineering Survey Institute of Shandong Province, which mainly tested the principal hydrochemical constituents in the water samples. The pH was measured using a pH meter (Hash, HQ40d), total dissolved solids (TDS) was determined by the weighing method (electronic balance, ME204E/02), and total hardness (TH) was calculated. Concentrations of major ions – $Na^+$, $K^+$, $Mg^{2+}$, $Ca^{2+}$, $SO_4^{2-}$, $Cl^-$, and $NO_3^-$ – were quantified by ion chromatography (Thermo Fisher, Aquion, USA), while $HCO_3^-$ was measured by titration

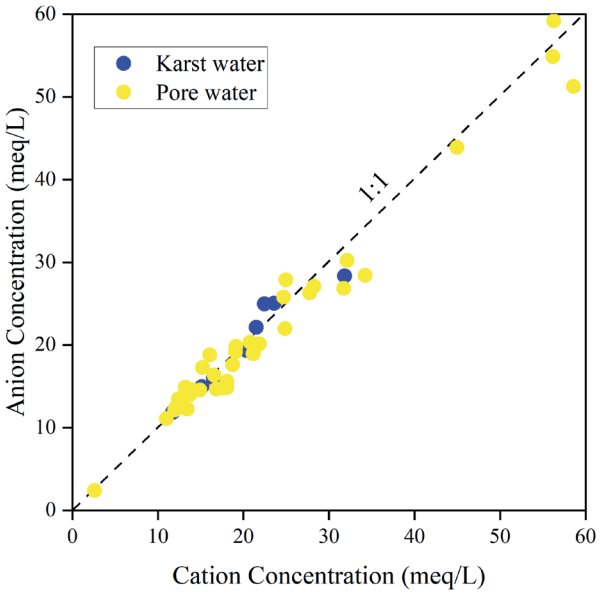


Fig. 3. Cation-to-anion ratio diagram.

(acid burette). To ensure data reliability, an ion balance check was performed on all samples prior to analysis. The results showed that the ion balance errors were within ±5% [20], confirming the accuracy and reliability of the data used in this study. Furthermore, in the cation-to-anion ratio diagram (Fig. 3), all water samples cluster near the 1:1 line, providing further corroboration of the ionic equilibrium.

### Methods of Analysis

This investigation utilized statistical methods and boxplot visualization to characterize and compare the fundamental hydrochemical properties of distinct groundwater classifications in SDLR. Groundwater hydrochemical facies were delineated through Piper trilinear plot analysis, with Gibbs diagrams and ionic proportional relationships employed to elucidate the dominant controlling mechanisms of water chemistry evolution. The basic statistical analysis of hydrochemical data was conducted using Excel, box plots were generated with Origin 2021, Piper plots were created using Aq·QA, and Gibbs and ion ratio plots were also produced in Excel. Additionally, Photoshop was employed for image processing and enhancement.

#### *Assessment of Irrigation Water Quality*

The sodium adsorption ratio (SAR) reflects the relative dominance of $Na^+$ in groundwater exchange reactions compared to other components (Equation (1)) [21, 22]. According to the USSL diagram, irrigation water is classified based on two criteria: Salinization Hazard (by EC): low (0~250), moderate (250~750), high (750~2250), or very high (> 2250); Alkalinity Hazard (by SAR): low (0~10), moderate (10~18), high (18~26), or extremely high (>26). By integrating these two

sets of criteria, a comprehensive classification system was developed, resulting in 16 distinct categories of irrigation water quality.

$$SAR=\frac{Na^+}{\sqrt{\frac{Ca^{2+}+Mg^{2+}}{2}}} \quad (1)$$

Percent sodium (%Na) serves as a reliable indicator for evaluating groundwater irrigation suitability (Equation (2)) [23]. Elevated $Na^+$ levels may adversely affect soil structure by decreasing permeability, and %Na is computed based on the formula below. The Wilcox plot characterizes both Na% and EC and is divided into a total of five zones, which are: excellent to good, good to permissible, permissible to doubtful, doubtful to unsuitable, unsuitable [21, 24].

$$\%Na=\frac{Na^+}{Ca^{2+}+Mg^{2+}+Na^+ +K^+}\times 100\% \quad (2)$$

*Evaluation of Drinking Water Quality*

The entropy weighted water quality index (EWQI) method was used to evaluate the suitability of drinking groundwater in the following steps (Equations (3-7)) [25]:

$$P_{ij}=\frac{y_{ij}}{\sum_{i=1}^{m} y_{ij}} \quad (3)$$

$$e_j=-\frac{1}{\ln m}\sum_{i=1}^{m} P_{ij}\ln P_{ij} \quad (4)$$

$$w_j=\frac{1-e_j}{\sum_{j=1}^{n}(1-e_j)} \quad (5)$$

$$q_j=\frac{C_j}{S_j}\times 100 \quad (6)$$

$$EWQI=\sum_{j=1}^{n} w_j q_j \quad (7)$$

Where, $P_{ij}$ denotes the standardized value for each parameter; $e_j$ represents the information entropy of individual factors; $w_j$ corresponds to the weighting coefficient; $q_j$ indicates the concentration ratio, $c_j$ signifies the measured concentration in sampled specimens, and $s_j$ adopts the standard concentration value of III water in the Groundwater Quality Standard (GB/T 148148-2017). Groundwater potability was categorized into five distinct classes according to EWQI values: excellent (0~25), good (25~50), moderate (50~100), poor (100~150), and very poor (150~200).

*Health Risk Assessment*

As an important resource for human survival, the amount of fluorine in groundwater is closely related to human health [21]. In the GB17018-1997 standard for the division of endemic fluorosis disease areas, the method of determining the endemic fluorosis disease areas in China and the division of the degree of the disease areas is clearly stipulated, and the appropriate interval of the quality concentration of fluorine in drinking water is 0.5~1.0 mg/L [21]. As a pervasive environmental issue, groundwater $NO_3^-$ contamination is particularly severe in regions with intensive agriculture. Given China's status as a major agricultural nation, the extensive use of nitrogen fertilizers and high irrigation demands have exacerbated $NO_3^-$ pollution in its agricultural basins [26]. To quantify the associated human health risks, we employed the U.S. Environmental Protection Agency's risk assessment model to evaluate the risks separately for adults and children [14, 21]. The computational expression is presented in Equations (8-14) [21]:

$$CDI=\frac{C_j\times IR\times EF\times ED}{BW\times AT} \quad (8)$$

$$DAD=\frac{DA_{event}\times EV\times ED\times EF\times SA}{BW\times AT} \quad (9)$$

$$DA_{event}=K_p\times C_j\times t_{event}\times 10^{-3} \quad (10)$$

$$HQ_{oral}=\frac{CDI}{RfD} \quad (11)$$

$$HQ_{der}=\frac{DAD}{RfD} \quad (12)$$

$$HI_i=HQ_{oral}+HQ_{der} \quad (13)$$

$$THI=\sum HI_i \quad (14)$$

CDI is drinking water intake (mg/kg/d); $C_j$ represents ion concentration (mg/L); IR denotes daily water consumption rate (L/d); EF signifies exposure frequency (d/a); ED indicates exposure duration (a); BW stands for average body weight (kg); and AT represents the mean exposure time (a) [21].

DAD is the exposure measure of groundwater under the dermal contact route (mg/kg/d), $DA_{event}$ is the absorbed dose during dermal contact (mg/cm$^2$), EV is the number of dermal contact events per day (times/d), SA is the surface area of exposed skin (cm$^2$), $K_p$ is the permeability coefficient of the hazardous substance (cm/h), $C_j$ is the concentration of the contaminant in groundwater (mg /L), and $t_{event}$ is the word skin contact duration. HQ is the non-carcinogenic risk factor; $HI_i$ is the non-carcinogenic risk index for a single pollutant i for all exposure routes; THI is the total non-carcinogenic risk index for n pollutants via all exposure routes [21]; RfD is the reference dose (mg/kg/d), with the RfD for $NO_3^-$ taken as 1.6 and that for $F^-$ taken as 0.06 [14].

The non-carcinogenic health risk assessment of SDLR groundwater was conducted by quantifying risk values across all exposure pathways and evaluating them against established reference thresholds. Per USEPA health risk assessment guidelines, the threshold value

for the target hazard index (THI) is established at 1.0. A THI exceeding this benchmark (THI>1.0) signifies that environmental exposure poses unacceptable non-carcinogenic health risks, whereas values below 1.0 (THI<1.0) indicate risk levels within the safe exposure limits.

## Results and Discussion

### Statistical Analysis of Water Chemistry

Statistical approaches facilitate characterization of fundamental hydrochemical properties of groundwater systems while elucidating their genetic mechanisms and evolutionary processes. The descriptive statistics of predominant ionic constituents in SDLR groundwater are presented in Table 1. The analysis revealed mean pH levels of 7.4 and 7.6 for karst water and pore water, respectively, demonstrating a weakly alkaline groundwater environment across the SDLR. In the SDLR, the TDS concentrations of karst water and pore water varied between 697-1,800 mg/L and 137-3,690 mg/L, with mean values of 1,268.88 mg/L and 1,264.08 mg/L, respectively. Similarly, TH levels ranged from 317-853 mg/L and 118-1,660 mg/L, averaging 622.88 mg/L and 1,660 mg/L, respectively. The mean values were 622.88 mg/L and 596.55 mg/L. Based on TDS and TH classification criteria, the predominant groundwater type in SDLR was identified as hard-saline water. In terms of mean values, the main anions and cations in karst water were $HCO_3^-$ (454.75 mg/L) and $Ca^{2+}$ (179.53 mg/L), respectively; while the primary cation in pore water was $Na^+$ with a mean value of 318.32 mg/L, and the main anion was $HCO_3^-$ with a mean value of 707.43 mg/L (Table 1). Comprehensive analysis revealed distinct ionic dominance patterns: in karst water, anion abundance followed $HCO_3^-$>$SO_4^{2-}$>$Cl^-$>$NO_3^-$ and cations $Ca^{2+}$>$Mg^{2+}$>$Na^+$>$K^+$, while pore water exhibited the same anion ordering but differed in cation dominance ($Na^+$>$Ca^{2+}$>$Mg^{2+}$>$K^+$).

### Hydrochemical Type

The Piper trilinear diagram [27] is a widely used method for water chemistry fractionation, with the advantage of being free from human influence [15]. The Piper diagram has a rhombus and two triangles, where the triangles show the relative proportions of anions and cations, and the rhombus demonstrates the overall hydrochemical characteristics [15, 18]. Fig. 4 presents the hydrochemical Piper diagrams, illustrating the distinct characteristics of various groundwater types within the SDLR. The hydrochemical analysis reveals distinct distributions for different water types. On the cation triangle diagram, samples are predominantly located in the central mixed zone. In contrast, on the anion triangle, they cluster near the $HCO_3^-$ end-member. When projected into the rhombus diagram, most samples fall within regions ① and ③, corresponding to the $HCO_3$-Ca·Mg and $SO_4$·Cl-Ca·Mg types, respectively. Karst water samples are primarily classified as $SO_4$·Cl-Ca·Mg (region ③), while pore water exhibits a more complex composition, spanning multiple regions but concentrating in regions ① and ③. This distribution confirms the previously documented anion evolution from $HCO_3$ to $SO_4$ and $SO_4$·Cl types during the transition from pore to karst water along the runoff pathway.

### Analysis of Factors Influencing Groundwater Hydrochemistry

#### *Weathering of Rocks*

Overall, the water chemical characteristics of groundwater are predominantly influenced by three key

Table 1. Statistical results of groundwater in SDLR.

| | Karst water | | | Pore water | | |
|---|---|---|---|---|---|---|
| | Max | Min | Mean | Max | Min | Mean |
| TDS mg/L | 1800 | 697 | 1268.88 | 3690 | 137 | 1264.08 |
| TH mg/L | 853 | 317 | 622.88 | 1660 | 118 | 596.55 |
| pH | 8.4 | 7.1 | 7.4 | 8.5 | 7.0 | 7.6 |
| $Ca^{2+}$ mg/L | 345 | 41.2 | 179.53 | 248 | 36.4 | 107.13 |
| $Mg^{2+}$ mg/L | 99.5 | 9.96 | 59.28 | 258 | 5.07 | 80.84 |
| $Na^+$ mg/L | 241 | 56.5 | 147.44 | 855 | 6.46 | 228.90 |
| $K^+$ mg/L | 4.07 | 0.13 | 2.24 | 11.5 | 0.16 | 1.72 |
| $HCO_3^-$ mg/L | 613 | 340 | 454.75 | 1080 | 123 | 707.43 |
| $SO_4^{2-}$ mg/L | 734 | 52.4 | 324.30 | 1240 | 11.1 | 250.80 |
| $Cl^-$ mg/L | 348 | 128 | 210.75 | 643 | 4.98 | 154.56 |
| $NO_3^-$ mg/L | 79.3 | 0.54 | 32.25 | 61.13 | 0.31 | 9.47 |

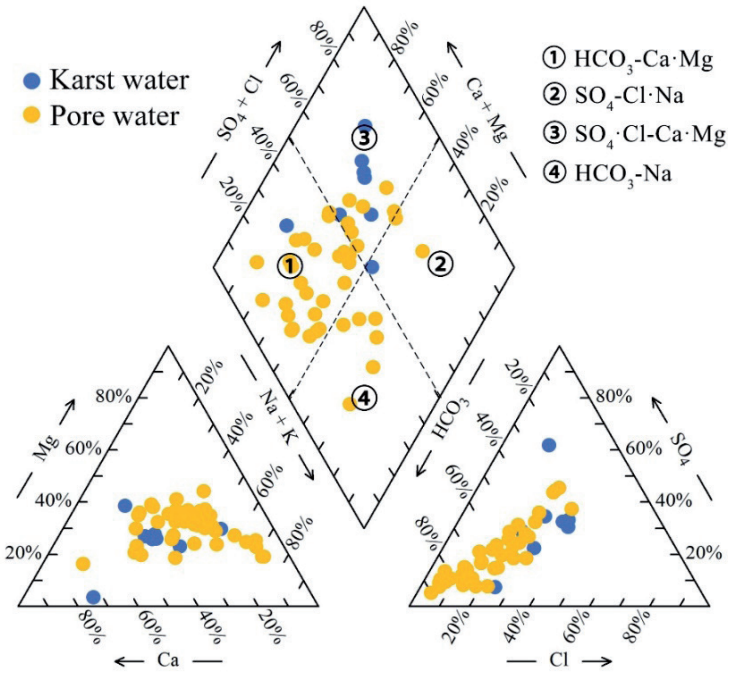


Fig. 4. Piper trilinear map of groundwater in the SDLR.

factors: rock weathering, atmospheric precipitation, and evaporative crystallization [15, 28, 29]. The Gibbs plot is a semi-logarithmic coordinate model that uses the mass concentration of TDS on the vertical axis and the ratios of the mass concentrations of $Na^+$ to $Na^+$+$Ca^{2+}$ and $Cl^-$ to $Cl^-$+$HCO_3^-$ on the horizontal axis [30]. In the Gibbs model, the middle to the left, the upper right, and the lower right represent the three control zones of rock weathering, evaporation and crystallization, and then atmospheric precipitation, respectively, as depicted in Fig. 5. This model is widely applied in the analysis of the hydrochemical genesis of groundwater [15, 28]. Projecting the groundwater sample points in the SDLR into the Gibbs model, the distribution of the water sample points is predominantly observed within the control area governed by rock weathering (Fig. 5).

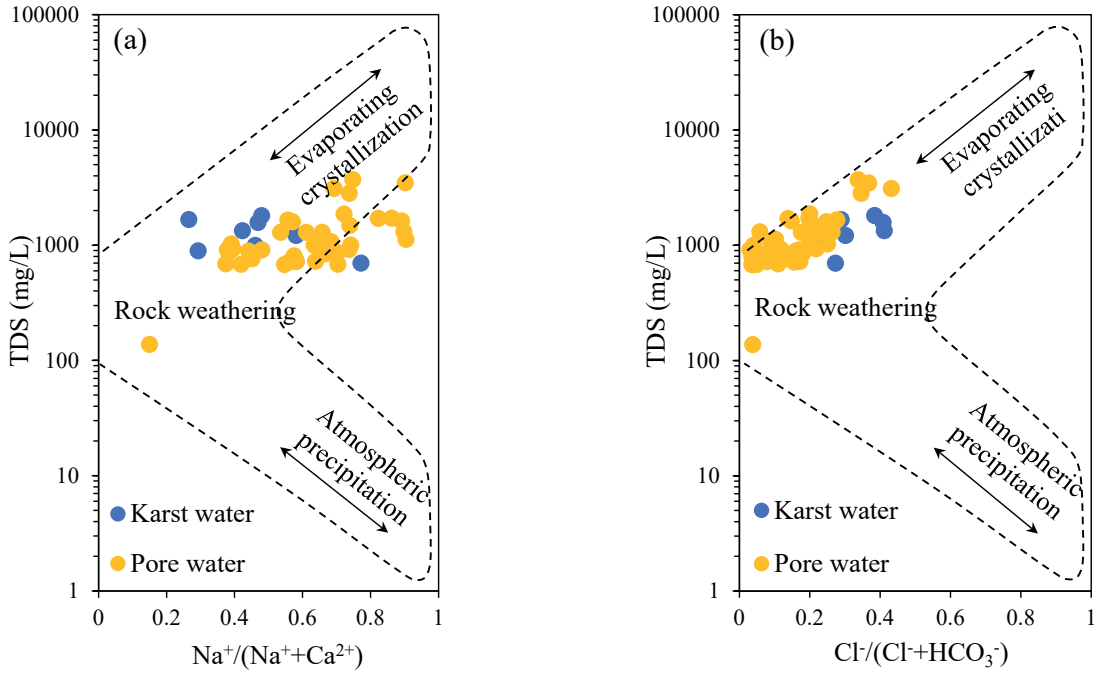


Fig. 5. Gibbs diagram of groundwater hydrochemistry in SDLR.

This pattern of distribution suggests that rock weathering is the primary factor shaping the hydrogeochemical signatures of groundwater in the SDLR.

The proportions of major ions in groundwater can serve as a basis for further elucidating the principal sources of these ions in groundwater [18, 31]. The dissolution of halite (NaCl) constitutes a substantial source of $Na^+$ and $Cl^-$ in groundwater. Consequently, from a theoretical standpoint, the ratio of $Na^+/Cl^-$ would be expected to approximate 1 if the primary origin of $Na^+$ and $Cl^-$ in groundwater is the dissolution of halite [4, 32]. A scatter plot showing the $Na^+$ to $Cl^-$ ratio in the groundwater of the SDLR is presented in Fig. 6a). It is noted that the majority of water sample points are predominantly located along the 1:1 line, suggesting that the $Cl^-$ in groundwater is not sufficient to fully counterbalance the $Na^+$. This suggests that salt rock dissolution is not the primary source of $Na^+$ and $Cl^-$ in groundwater. Furthermore, the surplus $Na^+$ could potentially stem from the dissolution of silicate rock minerals or from cation exchange reactions. Analogously, if the dissolution of gypsum ($CaSO_4 \cdot 2H_2O$) is the predominant source of $Ca^{2+}$ and $SO_4^{2-}$ in groundwater, the ratio of $Ca^{2+}$ to $SO_4^{2-}$ would be expected to be near 1 [13, 15]. As depicted in Fig. 6b), the distribution of groundwater sampling points in the SDLR primarily lies to one side of the 1:1 line, and some of them are close to the 1:1 line, which indicates that gypsum dissolution exists in the groundwater in the SDLR, but it is not the only source of $Ca^{2+}$ and $SO_4^{2-}$. Weathering of carbonate rocks is an important factor affecting $Ca^{2+}$and $HCO_3^-$ content in groundwater [18, 33].

Fig. 6c) shows the ratio relationship between $Ca^{2+}$and $HCO_3^-$ in groundwater in the SDLR, and it can be seen that most of the water sampling points are near to 1:1 line and 1:2 line or are located in the middle of the distribution of the two lines, which indicates that the carbonate rock mineral dissolution is the main source of $Ca^{2+}$and $HCO_3^-$ in groundwater in SDLR. The ratio of $(Ca^{2+}+Mg^{2+})$ to $(HCO_3^-+SO_4^{2-})$ is frequently employed to assess the influence of silicate rock, carbonate mineral, and gypsum dissolution on groundwater chemistry [15, 18, 33]. In Fig. 6c), a portion of the water sampling points lies below the 1:1 line, which may be related to agricultural activities within the SDLR. Certain fertilizers contain substantial amounts of $Ca^{2+}$, and fertilization practices often introduce both $NO_3^-$ and additional $Ca^{2+}$ simultaneously, thereby resulting in

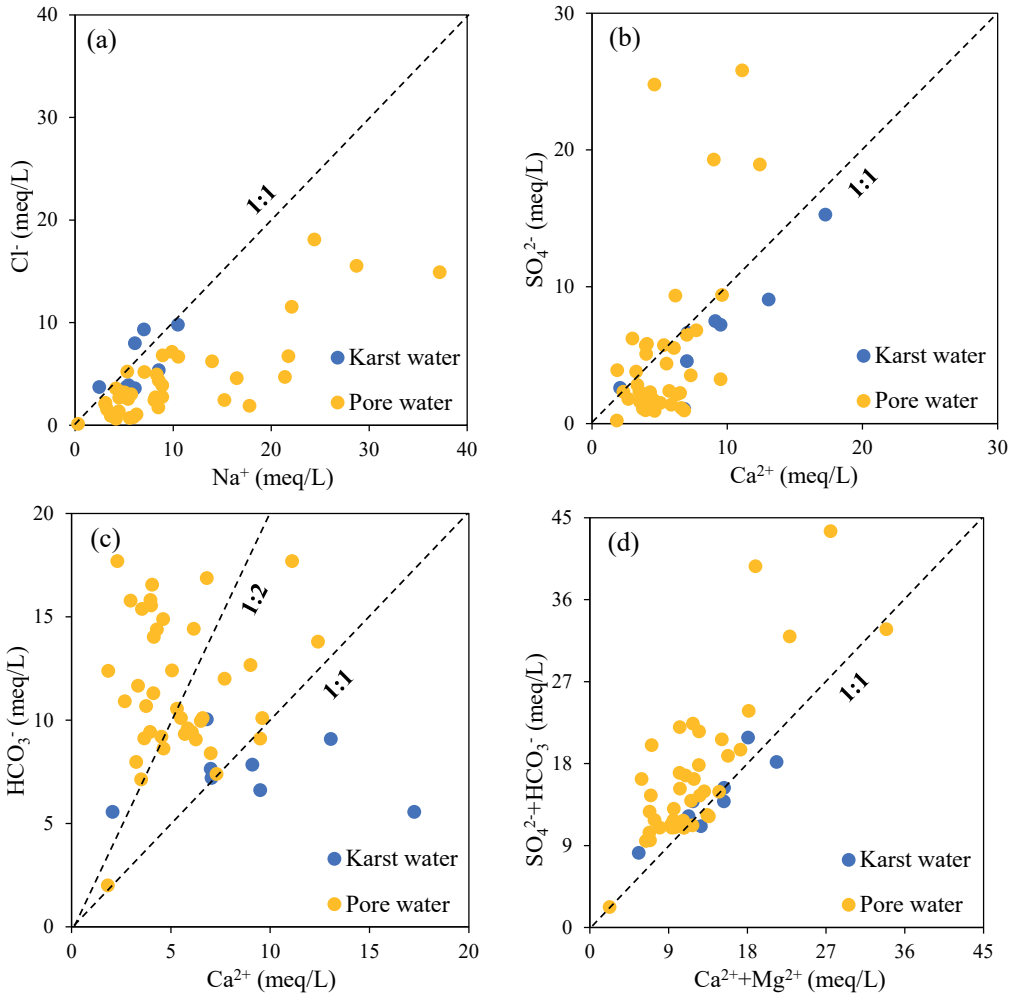


Fig. 6. Scatter plot of major ion ratios of groundwater in the SDLR.

this distribution pattern at the sampling points. Fig. 6d) illustrates that the majority of groundwater sampling points in the SDLR fall above the 1:1 line, with a few positioned along it. Such a trend underscores the predominant role of carbonate mineral weathering in shaping the region's groundwater chemical composition. Additionally, it suggests that there is also dissolution occurring from silicate rock minerals and gypsum.

*Cation Exchange*

Cation exchange typically represents another significant process governing groundwater chemical evolution in regional aquifers [15, 34]. The correlation between $Ca^{2+}$ + $Mg^{2+}$ - $HCO_3^-$ $SO_4^{2-}$ versus $Cl^-$ - $Na^+$ - $K^+$ can be used to identify the cation exchange process. A ratio approximating unity suggests cation exchange plays a substantial role in the groundwater system [34]. Fig. 7a) demonstrates that SDLR groundwater samples predominantly follow a 1:1 trend line. The regression equation (y = 0.9884x - 0.8455, $R^2$ = 0.8288) exhibits a slope approximating unity, indicating cation exchange significantly influences groundwater chemistry in southwestern Dongping Lake.

Additionally, the Chlor-alkali index (CAI) serves as a reliable indicator for ascertaining the direction of cation exchange processes [5], and the CAI calculation formula is shown in Equations (15) and (16). If the values of CAI-1 and CAI-2 are both negative, it indicates that forward cation exchange occurred, that is, Na in the aquifer was exchanged with $Ca^{2+}$ in the aqueous solution (Equation (17)); if the values of CAI-1 and CAI-2 are both positive, it indicates that reverse exchange has occurred, that is, $Ca^{2+}$ in the aquifer is exchanged with $Na^+$ in the groundwater (Equation (18)) [5]. Fig. 7b) demonstrates that the majority of SDLR groundwater samples plot in the CAI<0 domain, evidencing forward cation exchange wherein aquifer $Na^+$ is replaced by aqueous $Ca^{2+}$.

$$CAI-1=\frac{Cl^- - Na^+ - K^+}{Cl^-} \quad (15)$$

$$CAI-2=\frac{Cl^- - Na^+ - K^+}{HCO_3^- + SO_4^{2-} + CO_3^{2-} + NO_3^-} \quad (16)$$

$$2NaX + Ca^{2+} \rightarrow 2Na^+ + CaX_2 \quad (17)$$

$$2Na^+ + CaX_2 \rightarrow 2NaX + Ca^{2+} \quad (18)$$

The groundwater environment has become increasingly impacted by anthropogenic influences, particularly in regions experiencing substantial human activities, due to swift socio-economic growth, rapid urbanization, and population expansion [15, 34]. Groundwater nitrate primarily originates from industrial and agricultural operations, along with domestic wastewater effluents. $NO_3^-$ concentration levels can effectively reflect the degree of anthropogenic influence on groundwater systems [13]. Fig. 8 illustrates the concentrations of $NO_3^-$ in various types of groundwater within the SDLR. For karst water and pore water, the $NO_3^-$ concentrations varied between 0.54 mg/L and 79.30 mg/L, and between 0.31 mg/L and 61.13 mg/L, respectively. The mean concentrations were 32.25 mg/L for karst water and 9.47 mg/L for pore water. In most cases, $NO_3^-$ levels in SDLR groundwater remain below the Class III water quality threshold (88.57 mg/L) set by groundwater standards. This suggests that the groundwater is relatively less affected by anthropogenic inputs. In contrast, karst water is more significantly influenced by human activities than pore water. This is attributed to the shallow depth of karst water, which ranges from 20 to 30 meters, often shallower than the sampling depth of some pore water. Additionally, karst water is more extensively exploited and utilized, making its susceptibility to human inputs more pronounced.

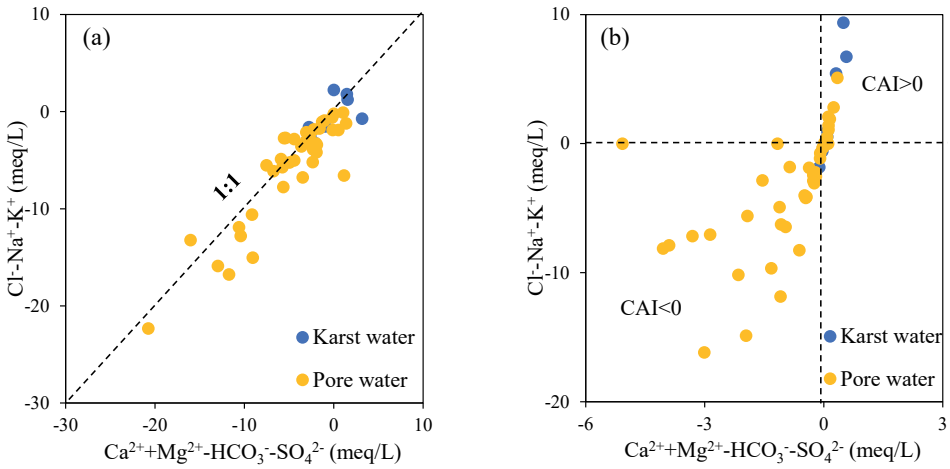


Fig. 7. $Ca^{2+}$+$Mg^{2+}$-$HCO_3^-$ $SO_4^{2-}$ vs. $Cl^-$ -$Na^+$-$K^+$ and CAI-1 vs. CAI-2 in groundwater in SDLR.

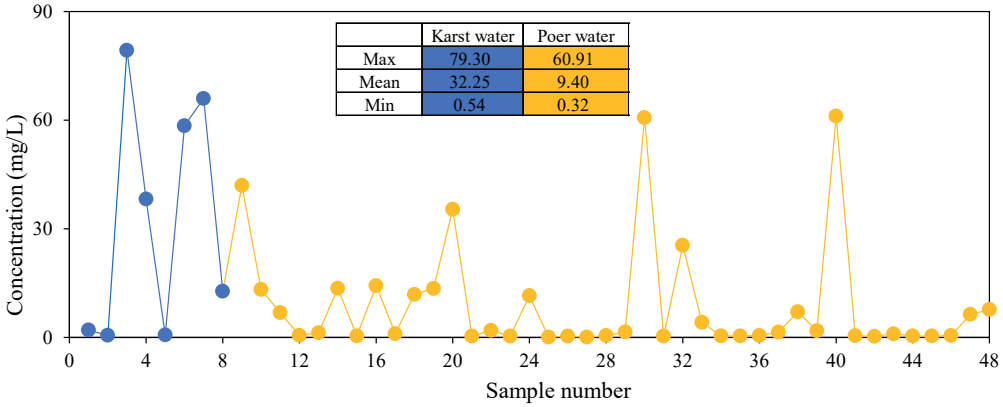


Fig. 8. Line graph of $NO_3^-$ concentration in groundwater in SDLR.

Determining the origins of nitrate in groundwater is essential for effective pollution prevention and control, as well as for the sustainable development, utilization, and management of groundwater resources. The ratios of $NO_3^-/Ca^{2+}$ and $SO_4^{2-}/Ca^{2+}$ are frequently employed to identify pollution sources, including industrial and mining effluents, agricultural runoff, and domestic sewage [7].

Fig. 9a) demonstrates that the water sampling points in the SDLR were predominantly aligned along the horizontal axis, suggesting that agricultural runoff and domestic wastewater were the primary sources of groundwater $NO_3^-$. In addition, $Cl^-$ is a conservative element that does not readily react in groundwater and can be used to indicate water pollution. If $Cl^-$ is contained in fertilizers, it increases with the increase of $NO_3^-$, while human and animal manure or domestic wastewater are usually characterized by high $Cl^-$ and low $NO_3^-$ [35, 36]. Therefore, the $NO_3^-/Cl^-$ value can be used to analyze the source of $NO_3^-$. Fig. 9b) presents the $Cl^-$ versus $NO_3^-/Cl^-$ scatter plot for SDLR groundwater, with sample clustering in the lower right quadrant suggesting feces and wastewater-derived nitrate as the dominant contamination source. During the field sampling process, it was noted that the use of farmyard fertilizer was prevalent, which aligns with the analysis that the $NO_3^-$ content in groundwater is closely linked to human and animal manure. Additionally, denitrification occurred in some water sample points during the migration of nitrogen through the soil with groundwater.

## Water Quality Evaluation

### *Irrigation Water Quality Assessments*

From the sodium adsorption ratio index, the vast majority of pore water and all karst water fall within the low alkalinity damage range, with only one pore water

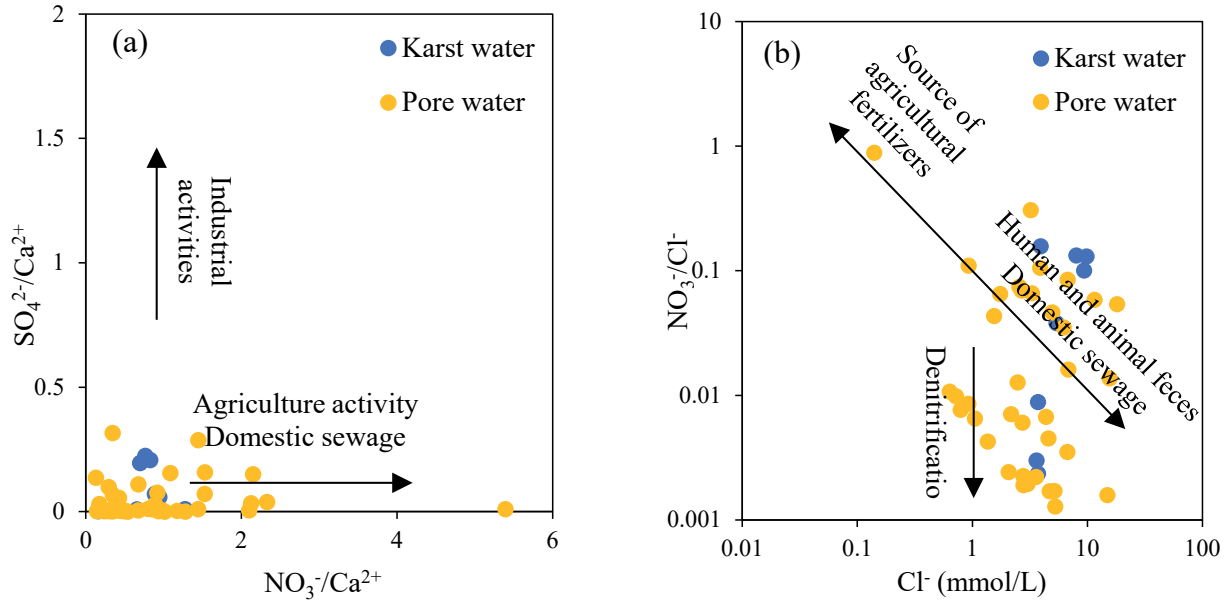


Fig. 9. Scatter plot of $NO_3^-/Ca^{2+}$ vs. $SO_4^{2-}/Ca^{2+}$ and $Cl^-$ vs. $NO_3^-/Cl^-$ in groundwater in the SDLR.

sample site in the moderate alkalinity damage range. These results demonstrate that the majority of SDLR groundwater meets agricultural irrigation standards without inducing substantial soil alkalization. Fig. 10a) reveals that karst aquifers are principally confined to the C3-S1 zone, exhibiting elevated salinity but limited alkaline properties. One karst water sample point is in a region of very high salinity, indicating that its conductivity is very high and it is unsuitable for irrigation. Pore water predominantly occurs within two distinct hydrochemical zones: the C3-S1 region and the C4-S2 region. A singular pore water sample located in the C4-S3 zone, displaying exceptionally high salinity and alkalinity, indicates compromised water quality, rendering it agriculturally unsuitable. Another pore water sample is in the C1-S1 region of low salinity and low alkalinity, indicating low conductivity, low sodium adsorption ratio, and very good water quality suitable for irrigation. In summary, karst action, such as the dissolution of carbonate minerals, may contribute to the increased conductivity of karst water, but the overall water quality is generally good. Pore water is widely distributed and may be influenced by local geological conditions, such as the dissolution of salt formations, or anthropogenic activities, such as agricultural irrigation and pollution, leading to significant variations in conductivity and sodium adsorption ratios.

Wilcox diagram analysis (Fig. 10b)) reveals that 50% of the eight karst water samples classify as 'good' quality, while the remaining 50% are in the water quality reserve category based on sodium percentage criteria. Quality assessment of the 40 pore water samples reveals the following distribution: 1 sample (2.5%) falls within the excellent category, 14 samples (35%) in the good category, 13 samples (32.5%) in the usable category, 7 samples (17.5%) in the permissible reserve category, and 5 samples (12.5%) in the unsuitable category. Overall, there is no salinity risk in the karst water samples from the SDLR, and these samples are suitable for irrigation. However, 12.5% of the pore water samples exhibit a serious salinity risk, suggesting that water samples from some areas within the study region are not suitable for irrigation.

### *Drinking Water Quality Assessments*

This study selected $Na^+$, $Cl^-$, $SO_4^{2-}$, $NO_3^-$, $F^-$, TDS, TH, and pH as evaluation factors. Results indicate that the EWQI values for water samples in the study area ranged from 19.95 to 272.24, with an average of 127.01. According to the EWQI classification, only 16.67% of samples in the study area were rated as excellent or good, indicating overall poor water quality. The majority of water samples (54.17%) were classified as poor or very poor, rendering them unsuitable for drinking. The EWQI distribution map (Fig. 11) intuitively shows that the green area (EWQI>150) is concentrated in the northern part of the study area, including 4 karst water samples and 12 pore water samples, while the water quality in the southern region is relatively good. Combined with the distribution of land use in SDLR, areas with poor water quality correspond to agricultural and urban land use, which indicates that agricultural and domestic wastewater discharge may lead to deterioration of water quality.

As data $NO_3^-$, $Cl^-$, $Na^+$, and others are not normally distributed, and the Spearman rank correlation coefficient does not directly utilize raw variable values but instead converts them into ranks, it is insensitive to outliers and does not require data to follow a normal distribution. Therefore, this study employs the Spearman rank correlation coefficient to derive the rank correlation coefficients between each parameter and the EWQI (Fig. 12b)). Variance contribution, or sensitivity analysis, was calculated by computing the squared values of the rank correlation coefficients and subsequently normalizing these values.

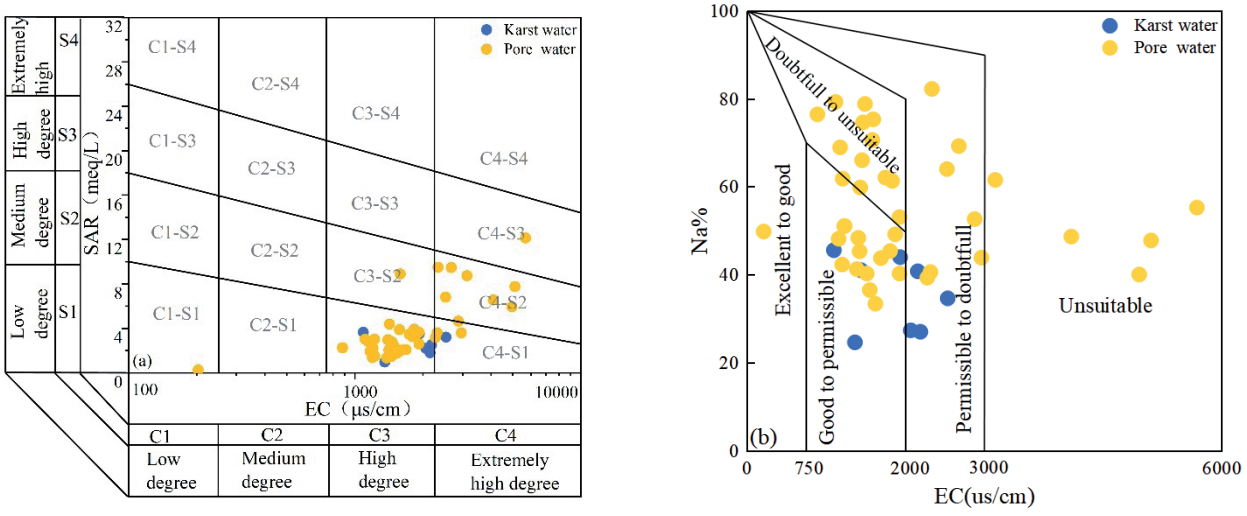


Fig. 10. Irrigation water quality assessment (a. USSL; b. Wilcox).

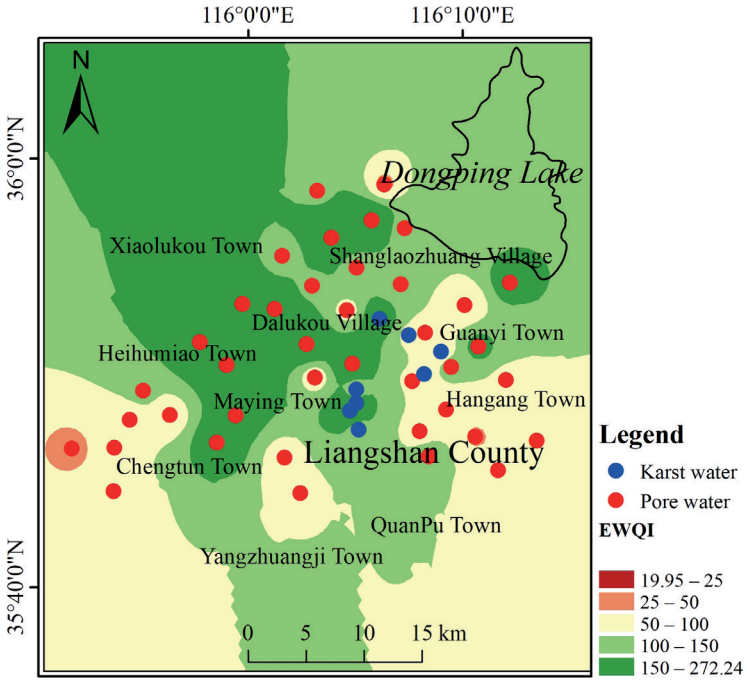


Fig. 11. EWQI distribution map in the SDLR.

As shown in Fig. 12, $NO_3^-$ is the dominant factor, contributing 87.6% of the prediction variance. The rank correlation coefficient of 0.89 indicates that there is a relatively strong positive monotonic relationship between $NO_3^-$ and EWQI, which means that the change of nitrate concentration plays a dominant role in the uncertainty of EWQI. $Cl^-$ contributes 11.3%, which is the secondary factor with substantial influence. The rank correlation coefficient of 0.32 indicates a moderate positive correlation. The contribution of $Na^+$, pH, $SO_4^{2-}$, TH, and TDS is less than 1%, and these characteristics have little effect on the variance of model prediction. The negative correlation (-1%) of TH is almost zero, indicating that there is almost no monotonic relationship.

## Health Risk Evaluation

An ecological risk assessment for human health is a method that evaluates the relationship between groundwater chemical components and human health. Local populations are primarily exposed to

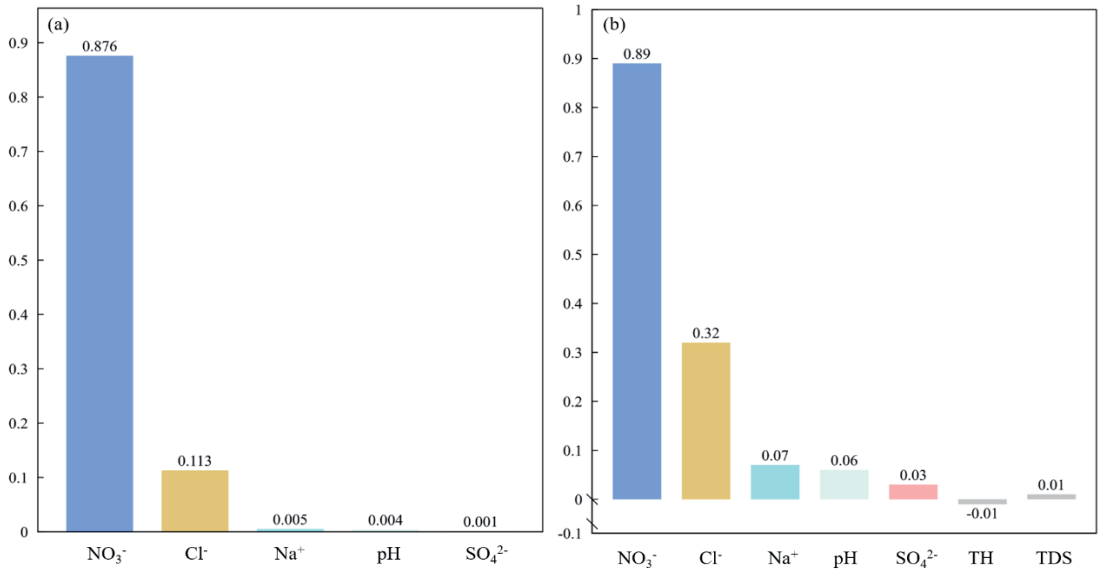


Fig. 12. a) Sensitivity analysis; b) Rank-related coefficient.

Table 2. Health risk hazard index statistics.

| Index | Exposure pathway | Adult | | | Children | | |
|---|---|---|---|---|---|---|---|
| | | Max | Min | Mean | Max | Min | Mean |
| $F^-$ | Oral | 1.74 | 0.01 | 0.50 | 4.07 | 0.02 | 1.17 |
| | Skin | 2.57 | 0.01 | 0.74 | 7.49E-03 | 4.43E-05 | 0.002 |
| | HQ | 4.08 | 0.02 | 1.18 | 4.31 | 0.03 | 1.24 |
| $NO_3^-$ | Oral | 1.20 | 1.52E-03 | 1.19 | 2.81 | 3.54E-03 | 0.45 |
| | Skin | 2.34E-03 | 2.95E-06 | 4E-04 | 5.17E-03 | 6.52E-06 | 8E-04 |
| | HQ | 1.21 | 1.52E-03 | 0.19 | 2.81 | 3.55E-03 | 0.45 |
| | HI | 4.44 | 0.12 | 1.44 | 5.09 | 0.13 | 1.63 |

contaminants through two pathways: drinking and dermal contact, especially through bathing. According to the descriptive statistics of groundwater in the SDLR, nearly half of the groundwater sample points have excessive fluoride content, which may pose health risks to humans. Therefore, this paper selects two indicators, $NO_3^-$ and $F^-$, for human health risk assessment. The non-carcinogenic risk index is obtained, and its characteristics are statistically calculated based on the evaluation indicators and exposure pathways. The results are presented in Table 2.

Table 2 demonstrates that non-carcinogenic risks were detected in 60.4% of the samples for both adults and children, with adults experiencing significantly lower non-carcinogenic risks compared to children. This disparity is primarily due to the fact that the non-cancer risk index is predominantly influenced by the ratio of average daily exposure dose to body weight, which varies among different exposure groups. A higher ratio correlates with a greater risk. As indicated in Table 2, the non-cancer risk associated with oral intake is higher than that from dermal contact, suggesting that oral intake is the primary exposure pathway contributing to non-carcinogenic risks.

Furthermore, this study also assessed non-carcinogenic health risks based on the daily water consumption reference values provided by the WHO. HI (Hazard Index) results indicate that, based on parameters provided by the WHO, the non-carcinogenic risk for adults and children has risen to 68.75% and 72.92%, respectively, while the mean values have increased from 1.44 and 1.63 to 1.67 and 1.91. Both exceed the HI threshold. This demonstrates that WHO parameters may not be universally applicable across all regions.

From Fig. 13, it can be seen that the distribution of areas where both adults and children have an HI greater than 1 for $F^-$ is largely similar, primarily in the northern and southwestern parts of the SDLR. The most severely affected location is Yangzhuang Jitian, where the impact is widespread, affecting almost the entire town's population of adults and children. Children exhibit significantly higher mean HI values compared to adults, suggesting that fluoride presents an elevated non-carcinogenic health risk to the pediatric population. Furthermore, the spatial distribution of high and low non-carcinogenic risk levels associated with nitrate exposure demonstrates comparable patterns between adults and children. The low-value areas are mainly located in the eastern and central parts of the SDLR, particularly in Hangang Township, Tuanyi Township, Dailukou Township, Maying Township, and Heihumiao Township. The spatial characteristics of HI are further elucidated by SDLR land use. The pronounced HI values in the northwestern and southern regions are attributable to the extensive farmland use there, presenting a marked agricultural signature. Conversely, the central and eastern areas, characterized by construction and a lake, correspond to zones of diminished HI. When integrated with the data presented in Table 2, the analysis reveals that the mean HI for children exceeds that of adults by a factor of 2.3, indicating significantly higher exposure levels and a more extensive spectrum of nitrate-induced non-carcinogenic health risks in the pediatric population. Furthermore, comparative risk assessment demonstrates that $NO_3^-$ exhibits a higher mean non-carcinogenic risk than fluoride, with the maximum risk value for children surpassing that observed in adults. Regarding exposure pathways, oral ingestion is the primary route affecting health risks, significantly higher than the risks posed by dermal contact.

## Sustainable Management of Groundwater Resources

Groundwater serves as the primary source of drinking and production water in the study area, playing a crucial role in supporting daily life, industrial production, and agricultural development [20]. To ensure effective management and utilization of groundwater resources and to achieve their sustainable use [20], the following measures are proposed:

(1) The results showed that nitrate in SDLR mainly came from agricultural activities and domestic sewage. The local government should set up groundwater monitoring wells around agriculturally intensive areas and villages, focusing on monitoring

the spatial and temporal changes of nitrate concentration, and combining isotope technology to trace the contribution rate of pollution. The high-risk areas of nitrate were delineated, and targeted measures such as agricultural fertilizer limitation and priority transformation of sewage pipe network were implemented.

(2) For the phenomenon that the risk of groundwater salinity in some areas is serious, low-salinity surface water can be preferentially used to replace high-salinity groundwater irrigation through the South-to-North Water Diversion Project or the surface water diversion canal system of Dongping Lake to reduce the dependence on groundwater. The soil-

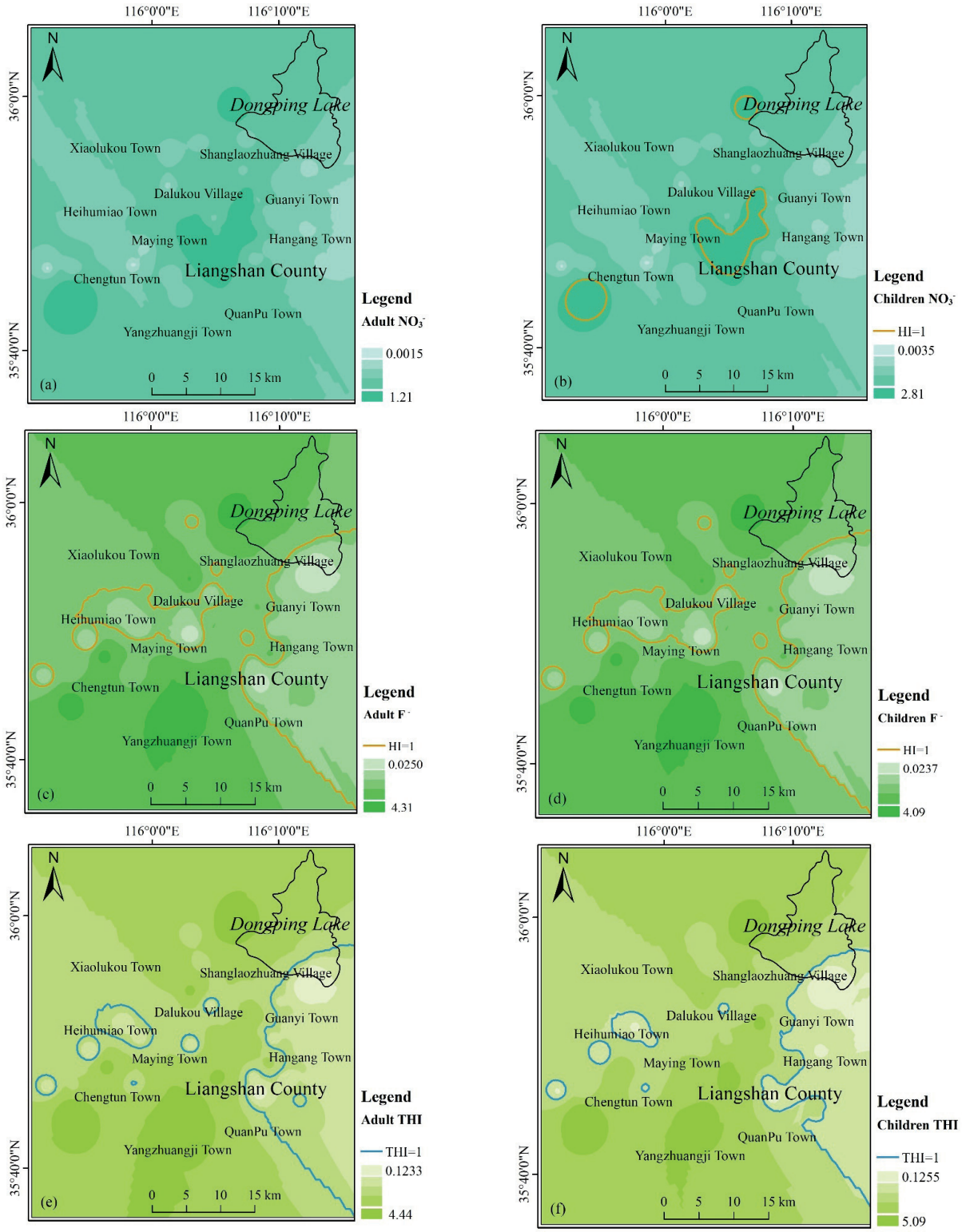


Fig. 13. Spatiotemporal distribution patterns of health risks associated with groundwater exposure.

groundwater salinity joint monitoring network was set up, and the conductivity sensor and remote sensing inversion technology were used to monitor the spatial distribution of salinity in real time and identify the risk area. Zhang et al. used a calibrated model to predict the changes in water level and $NO_3^-$ concentration over the next 30 years in three different scenarios. The prediction results show that if no measures are taken, the concentration of $NO_3^-$ in groundwater will further increase. In view of this, the first measure taken is to control the emissions of pollution sources, especially surface pollution sources; the second is to choose sites with severe pollution for pollution remediation [37].

(3) Given children's heightened vulnerability to environmental contaminants, protective interventions must be prioritized. These should include: ensuring safe water supplies in schools and playgrounds; implementing routine pediatric health screenings with emphasis on hematological and gastrointestinal parameters to monitor nitrate exposure effects; and strengthening health literacy programs targeting both youth and caregivers to foster safe water practices and discourage consumption of untreated groundwater.

(4) Managers should rationally plan groundwater resources and strictly control groundwater exploitation; strengthen pollution prevention and control; promote the application of scientific and technological innovation in groundwater management.

## Conclusions

(1) The mean pH values of karst water and pore water in the southwestern part of Dongping Lake were 7.4 and 7.6, respectively, indicating an overall weakly alkaline environment. The average values of TDS and TH were 1,268.88 mg/L and 1,264.08 mg/L, respectively. Most of the water samples were classified as hard-saline water. The main ions of karst water were characterized by $Ca^{2+}>Mg^{2+}>Na^{+}>K^{+}$ and $HCO_3^-> SO_4^{2-} >Cl^->NO_3^-$, whereas the pore water existed in the order of $Na^{+}>Ca^{2+}>Mg^{2+}>K^{+}$ and $HCO_3^-> SO_4^{2-} >Cl^->NO_3^-$.

(2) Hydrochemical analysis reveals distinct groundwater facies, with karst aquifers exhibiting dominant $SO_4$·Cl-Ca·Mg water types, while pore waters predominantly classify as $HCO_3$-Ca·Mg and $SO_4$·Cl-Ca·Mg. Geochemical evolution is principally governed by rock-water interactions, particularly the weathering of carbonate and silicate mineral assemblages along with gypsum dissolution. Furthermore, hydrochemical signatures in SDLR aquifers are significantly influenced by cationic exchange processes.

(3) The $NO_3^-$ content in the groundwater in SDLR is relatively low, and none of the water samples exceeded the limit of Class III water in the standard. Its main sources are human and animal feces and domestic sewage, while denitrification has occurred in some of the water sample points. In addition, karst water is more obviously affected by anthropogenic inputs than pore water.

(4) The SAR calculations suggest that the risk of salinization exceeds that of alkali damage in the SDLR. Additionally, the % Na analysis indicates no risk of salt-alkali hazards in the karst water samples, making them suitable for irrigation. Notwithstanding the general suitability of most groundwater samples in the SDLR for irrigation applications, approximately 12.5% of pore water samples demonstrate substantial saline-alkali hazards. Spatial analysis reveals that severely contaminated drinking water sources are predominantly concentrated in the northern sector of the study area, comprising 4 karst aquifer samples and 12 pore water samples that fail to meet potability standards. In contrast, groundwater with moderate water quality is predominantly found in the southern part of the SDLR. Sensitivity analysis results indicate a strong positive monotonic relationship between $NO_3^-$ and EWQI, with nitrate concentration playing a dominant role in the uncertainty of EWQI values.

(5) Both adults and children are exposed to non-carcinogenic health risks in 60.4% of the samples, with adults experiencing significantly lower risks than children. The primary route of exposure to these non-carcinogenic risks is through oral intake. The distribution chart of the total risk index indicates that high-risk areas are predominantly situated in the northern and southwestern regions of the SDLR.

## Acknowledgments

We are grateful to the reviewers and editors for their valuable comments on this article. We gratefully acknowledge the financial support from the Shandong Province 2023 Ministerial and Provincial Agreement Geological Exploration Project, grant number [SDGP370000000020230201263A22 001], and also funded by Open Fund Project of Lunan Institute, grant number [DKJS202304].

## Data Availability statement

The data that support the findings of this study are available on request from the corresponding author. The data are not publicly available due to privacy or ethical restrictions.

## Conflict of Interests

The authors declare no conflict of interest.

## Author Contribution Statement

Feng Zhang: Formal analysis, software, methodology, writing-original draft. Bin Gao: Supervision, writing-original draft. Xia Chunying: Research, conceptualization, methodology, writing review, resource acquisition. Ren Lei: Investigation, resource acquisition. Yan Yalei: Investigation, resource acquisition. Xiao Hua: Writing review. Zheng Huiming: Investigation. All the authors have read and agreed to the published version of the manuscript.

## References


1. KIEU L., NGUYEN P. Groundwater Quality Assessment in the Middle-Upper Pleistocene Aquifer. Civil Engineering Journal. **10** (7), 2357, **2024**.
2. PHAM N., NGUYEN G. Evaluating Groundwater Quality Using Multivariate Statistical Analysis and Groundwater Quality Index. Civil Engineering Journal. **10** (3), 699, **2024**.
3. WANG P., ZHANG W., ZHU Y., LIU Y., LI Y., CAO S., HAO Q., LIU S., KONG X., HAN Z. Evolution of groundwater hydrochemical characteristics and formation mechanism during groundwater recharge: A case study in the Hutuo River alluvial–pluvial fan, North China Plain. Science of The Total Environment. **915**, **2024**.
4. MA N., GAO L., GE Z., LI M. Hydrochemical characteristics of groundwater in a plain river network region: Establishing linkages between source and water quality variables. Chemosphere. 138809, **2023**.
5. AJAYKUMAR V., MONDAL N.C. Hydrochemical Characteristics of Groundwater Resources and Its Importance in the Assessment of Rural Water Supply in Southern India. Bulletin of Pure & Applied Sciences-Geology. **42F** (1), **2023**.
6. UTAMAT W., INDRIANI R., HERMANA M., ANJASMARA I., GARINI S., PUTRA D. Towards Improving Sustainable Water Management in Geothermal Fields: SVM and RF Land Use Monitoring. Journal of Human, Earth, and Future. **5** (2), 216, **2024**.
7. DENG L., LU L., YUAN D., WANG J., FANG H. Groundwater chemical characteristics and water quality evaluation in river basins of Dongjiang and Hanjiang. Environmental Science & Technology. **47** (4), **2024**.
8. LIU J., GAO Z., WANG M., LI Y., MA Y., SHI M., ZHANG H. Study on the dynamic characteristics of groundwater in the valley plain of Lhasa City. Environmental Earth Sciences. **77** (18), 646, **2018**.
9. MA Y., YANG J., XU S. Chemical Characteristics and Genesis Analysis of Shallow Groundwater in Yanhe Town, Yuxi City. Journal of Kunming University of Science and Technology (Natural Science). **49** (2), 129, **2024** [In Chinese].
10. ESMAEILI-VARDANJANI M., RASA I., YAZDI M., PAZAND K. The hydrochemical assessment of groundwater resources in the Kadkan basin, Northeast of Iran. Carbonates and Evaporites. **31** (2), 129, **2015**.
11. ROSENTHAL E., ZILBERBRAND M., LIVSHITZ Y. The hydrochemical evolution of brackish groundwater in central and northern Sinai (Egypt) and in the western Negev (Israel). Journal of Hydrology. **337** (3-4), 294, **2007**.
12. LI X., HUANG X., ZHANG Y.H. Spatio-temporal analysis of groundwater chemistry, quality and potential human health risks in the Pinggu basin of North China Plain: Evidence from high-resolution monitoring dataset of 2015-2017. Science of The Total Environment. **800** (15), 149568, **2021**.
13. BISWAS T., PAL S.C., SAHA A. Hydro-chemical assessment of coastal groundwater aquifers for human health risk from elevated arsenic and fluoride in West Bengal, India. Marine Pollution Bulletin. **186**, 114440, **2023**.
14. EMERGENCY U.S.E.P.A.O.O., RESPONSE R. Risk Assessment Guidance for Superfund: pt. A. Human health evaluation manual. Office of Emergency and Remedial Response, US Environmental Protection Agency, **1989**.
15. LIU J., PENG Y., LI C., GAO Z., CHEN S. Characterization of the hydrochemistry of water resources of the Weibei Plain, Northern China, as well as an assessment of the risk of high groundwater nitrate levels to human health - ScienceDirect. Environmental Pollution. **2020**.
16. DIN I.U., ALI W., MUHAMMAD S., SHAIK M.R., SHAIK B., REHMAN I.U., TOKATLI C. Spatial distribution and potential health risk assessment for fluoride and nitrate via water consumption in Pakistan. Journal of Geochemical Exploration. **259**, **2024**.
17. ZHAO Q., LI Q., CHEN H., AN M., GAO X., ZHANG Y., HUANG H., SHI R., MAN W., WANG N. Analysis on hydrochemical characteristics and formation of groundwater in Liangshan county, Shandong Province. Journal of China Hydrology. **42** (2), 102, **2022** [In Chinese].
18. HU X., LI B., ZHANG B., YANG Y., CAI X., GONG X., XIANG X., WU T. Hydrochemical analysis and quality comprehensive assessment of groundwater in the densely populated coastal industrial city. Journal of Water Process Engineering. **63**, **2024**.
19. QIN N., CHENG W., DONG F., SUN J., HUANG W., CHENG L., HAO G. Chemical characteristics and quality evaluation of groundwater in Dongping Lake Area. Science Technology and Engineering. **22** (24), 10434, **2022** [In Chinese].
20. ZHANG M., HAN S., WANG Y., WANG Z., LI H., WANG X., LIU J., LI C., GAO Z. Characteristics and controlling factors of groundwater hydrochemistry in Dongzhi Tableland area of the Loess Plateau of eastern Gansu – A case study of Ning County area, north China. Water. **14** (22), 3601, **2022**.
21. ZHAO Z., GAO Z., LIU J., LUO Z., SUN H., WANG Y., LI F. Hydrochemical characterization and comprehensive water quality assessment of groundwater within the main stream area of Yishu River. Environmental Monitoring & Assessment. **196** (6), **2024**.
22. ZAIDI F.K., MOGREN S., MUKHOPADHYAY M., IBRAHIM E. Evaluation of groundwater chemistry and its impact on drinking and irrigation water quality in the eastern part of the Central Arabian graben and trough system, Saudi Arabia. Journal of African Earth Sciences. **120**, 208, **2016**.
23. TODD D.K., MAYS L.W. Groundwater hydrology. John Wiley & Sons, **2004**.
24. WILCOX L. Classification and use of irrigation waters. US Department of Agriculture, **1955**.
25. NATH A.V., SEKAR S., ROY P.D. Drinking and irrigation quality and pollution assessments of the groundwater resources from Alappuzha in Kerala(India)through an integrated approach using WQI and GIS. Journal of

Geochemical Exploration: Journal of the Association of Exploration Geochemists. 258, **2024**.
26. PENG H., YANG W., FERRER A.S.N., XIONG S., LI X., NIU G., LU T. Hydrochemical characteristics and health risk assessment of groundwater in karst areas of southwest China: A case study of Bama, Guangxi. Journal of Cleaner Production. **341**, 130872, **2022**.
27. PIPER A.M. A graphic procedure in the geochemical interpretation of water-analyses. Neurochemistry International. **6** (1), 27, **1984**.
28. XIA L., YOU H., LIU J., HAN C., GAO Z., PENG Y., LI C. Hydrochemical characteristics and water quality evaluation of groundwater in coastal area of Jiaodong Peninsula.Environmental Science & Technology. **44** (10), 1, **2021** [In Chinesse].
29. FENG G., LIU B., XU J., XU C, LUO J., WANG J. Characteristics and causes of shallow groundwater salinization in Juye County, Shandong Province. Journal of University of Jinan (Science and Technology). **38** (3), 257, **2024** [In Chines].
30. GIBBS R.J. Mechanisms controlling world water chemistry. Science. **170** (3962), 1088, **1970**.
31. UK M., JEMCOV I., MLADENOVI A., ILI M.O. Hydrochemical impact of the hydraulic tunnel on groundwater in the complex aquifer system in Pirot, Serbia. Carbonates and Evaporites. **35** (2), **2020**.
32. AGHAZADEH N., CHITSAZAN M., GOLESTAN Y. Hydrochemistry and quality assessment of groundwater in the Ardabil area, Iran. Applied Water Science. 1, **2016**.
33. ZONGJUN G., ZHIPENG W., KEQIANG H., KUZIN V., JIUTAN L. Hydrochemical characteristics and controlling factors of karst groundwater in middle and upper reaches of Dawen River basin. Bulletin of Geological Science and Technology. **41** (5), 264, **2022**.
34. MASOUD A.M., EL-MAGD S.A.A. Integration of hydrochemical and isotopic characteristics for identifying groundwater recharge sources of the Eocene carbonate aquifer, Western Desert, Egypt. Journal of African Earth Sciences. **187**, 104449, **2022**.
35. WU T., YUAN L., HAN S., LI F. Temporal and spatial distribution characteristics and origin analysis of nitrate pollution in groundwater in Angulinao inland river basin. Environmental Chemistry. **40** (8), 2515, **2021**.
36. HE J., MAO H., XUE Y., LIAO F., GAO B., RAO Z., YANG Y., LIU Y., WANG G. Variability in spatiotemporal groundwater nitrate concentrations in the northeast Ganfu Plain. Earth Science Frontiers. **31** (3), 360, **2024** [In Chinese].
37. ZHANG C., MA L.,ZHANG S.,LI Z.,YIN M., ZANG Y. The Application of Visual Modflow to the Simulation ofGroundwater Nitrate Contamination in Shifjiazhuang. Acta Geoscientica Sinica. (6), 561, **2007**.